

Shallow landslides stability evaluation in loess areas according to Revised Infinite Slope Model: A case study of the 2013 “7.25” Tianshui sliding-flow landslide in Gansu province, China
~~A novel prediction method for shallow landslides in loess areas: A case study of the 2013 “7.25” Tianshui sliding-flow landslide in Gansu province, China~~

5 Jianqi Zhuang¹, Jianbing Peng¹, Chenhui Du¹, Yi Zhu², Jiayu Kong¹,

¹College of Geological Engineering and Geomatics/Key Laboratory of Western China Mineral Resources and Geological Engineering, Chang’an University, Xi’an, Shaanxi, 710054, China

²College of Land Engineering, Chang’an University, Xi’an, Shaanxi, 710054, China

Correspondence to: Jianqi Zhuang (jqzhuang@chd.edu.cn)

10 **Abstract.** Shallow loess landslides induced by prolonged heavy rainfall are common in loess dominated areas and often result
in property loss, human casualties, and sediment pollution. Building a suitable prediction model for shallow landslides in loess
areas is critical for landslide mitigation. In 2013, prolonged heavy rains from July 19th to the 25th triggered mass sliding-flow
loess landslides in Tianshui, China. Landslide data, along with the characteristics of the sliding-flow loess landslides were
15 obtained through multiple field investigations and remote sensing interpretations. The sliding-flow loess landslides event
demonstrated clustering, high density, small areas, and long travel distance. The depth of the sliding surface correlates with
the saturated layer (i.e., liquid limited water content) arising from rainfall infiltration, with a sliding depth that is typically less
than 2 m and is negatively correlated with the slope. Based on the common characteristics of shallow loess landslides, the
mechanisms involved in the sliding flow landslide are proposed. The Revised Infinite Slope Model (RISM) was proposed
20 using an equal differential unit method to correct for deficiencies when the safety factor is unchanging or increases with
increasing slope, when greater than 40° as calculated using the Taylor slope infinite model. The relationship between the
critical depth and the slope of the shallow loess landslide was determined. The intensity-duration (*I-D*) prediction curve of the
rainfall-induced shallow loess landslides for different slopes was constructed and combined with the characteristics of rainfall
infiltration for use in forecasting regional shallow loess landslides. Additionally, the influence of loess strength on the shallow
loess landslide stability has been analysed. The shallow loess landslide stability responds to slope and cohesion but is not
25 sensitive to the internal friction angle.

1 Introduction

Loess is a porous and loose aeolian deposit of silt-sized particles mainly formed during the Quaternary period, and it is widely
distributed in Asia, Europe, North America, and South America (Li et al., 2020). In China, loess is widely distributed, with an
area of 630,000 km², accounting for 6.63% of the total land area in northwest, north, and northeast China. The loess deposit is

30 very deep, up to 300 m, and the integrity and continuity of the loess layers are the greatest in the world (Liu, 1985). However, loess dominated environments are extremely fragile, with substantial soil erosion, topographical variation, and subject to concentrated rainfall, and have now become one of the most developed geohazard areas in China (Derbyshire, 2001; Zhang and Liu, 2010; Zhuang et al., 2018). Loess creates unique soil with large pores, high compressibility, strong collapsibility, and high-water sensitivity, making it prone to surface failure (Xu et al., 2014; Li et al., 2007; Peng et al., 2015; Juang et al., 2018; 35 Zhuang et al., 2022). The key factor in triggering loess failure is the interaction between water and loess, which can destroy the loess structure and reduce its mechanical strength. In more than 85% of loess landslides, water is the key factor, displaying the characteristics of small early deformation, long run-out distance, location unpredictability, rapid occurrence, and liquefaction, resulting in serious property damage and human casualties (Dijkstra, 1995; Wang et al., 2014; Zhuang et al., 2018; Zhu et al., 2022).

40 Rainfall-induced slope failures are a common form of shallow landslides in the Chinese Loess Plateau (CLP). Field investigations revealed that more than 50,000 landslides have occurred in the loess plateau in recent decades (Zhuang et al. 2018; Zhuang et al., 2022). Most of those landslides were triggered by prolonged heavy rainfall and with a slip surface depth of no more than 2 m (Zhuang et al., 2017; Zhuang et al., 2018; Zhuang et al., 2022). Precipitation infiltrates into the soil and percolates through the loess to approximately 2 m, attributed to the decreased infiltration rate with increasing depth (Tu et al., 45 2009; Xu et al., 2011; Zhuang et al., 2018). Shallow loess landslide events, due to prolonged heavy rainfall, mostly occurred as sliding-flow landslides, occurring in northern Shaanxi and Tianshui in 2013, Tianshui in 2015, and northern Shaanxi in 2017 (Peng et al., 2015; Wang et al., 2015; Zhuang et al., 2017; Zhang et al., 2020). Another consequence of these landslides is that substantial amounts of sediment were transported into rivers in the area, polluting rivers, raising the riverbeds, and increasing flooding.

50 Many scholars have studied rainfall infiltration, landslide mechanisms, and forecasting rainfall-induced shallow landslides. Among them, the prediction of shallow loess sliding-flow landslides due to rainfall is the most common, as this information can be used for geohazard mitigation (Brenning, 2005; Bordoni et al., 2015; Ahmadi-adli et al., 2017; Reichenbach et al., 2018; Thomas et al., 2018; Cogan and Gratchev, 2019; Berti et al., 2020; Bordoni et al., 2020). Shallow landslide forecasting can be divided into three categories based on the prediction method. (1) Early warning of landslides through 55 monitoring time-based deformation data is an important forecasting tool (von Ruetze et al., 2011; Galve et al., 2015; Roccati et al., 2018; Segoni et al., 2018; Lombardo et al., 2020; Marino et al., 2020). Most landslide failure processes progress through deformation stages that gradually develop into a catastrophic failure. During this process, deformation is easily observed and monitored and is considered the most important factor for landslide prediction. This approach is most relevant for large-scale landslides which have obvious early deformation trends. Common approaches include (2) Landslide forecasting can also include temporal and spatial rainfall monitoring (Giannecchini, 2006; Salciarini et al., 2006; De Vita et al., 2012; Giannecchini et al., 2012; Cevasco et al., 2013; von Ruetze et al., 2013; Stähli et al., 2015). Rainfall is a key inducing factor of geohazards, and researchers have studied the critical rainfall values for intensity, duration, and total rainfall within specific areas for 60 predicting landslides. (3) Statistical and qualitative methods to evaluate landslide susceptibility, associated with landslide

occurrence, can yield maps showing landslide hazard zones which is useful for land use management and long-term predictions
65 (Jia et al., 2008; Zizioli et al., 2013; Cevasco et al., 2014; Goetz et al., 2015; Guzzetti et al., 2006; Di Napoli et al., 2020; Di
Napoli et al., 2021; Keles and Nefeslioglu, 2021). However, it is important to note that statistical method results are largely
dependent on the quality of data and the specific method used. (4) Landslide early warning and forecasting can also be based
on physical modelling (Montgomery and Dietrich, 1994; Montrasio and Valentino, 2007; Formetta et al., 2016; Schilirò et al.,
2016; Lizarrag et al., 2017; Wang et al., 2020; Leonarduzzi et al., 2021). Researchers have focused their efforts on elucidating
70 the mechanisms and conditions which lead to soil failure. The data for analysis comes from soil tests, deriving evidence of the
decay of cohesiveness and angles with precipitation infiltration (Skempton 1985; Iverson 2000; Baum et al. 2008; Baum and
Godt 2010; Medina et al., 2021), and quantitative landslide assessment. Several physically based models have been proposed,
including steady-state hydrology (SHALSTAB and SINMAP) (Montgomery and Dietrich, 1994; Pack et al. 1999), quasi-
steady hydrology (dSLAM, IDSSM) (Dhakal and Sidle 2003), and Transient hydrology (TRIGRS) (Iverson, 2000; Baum et
75 al. 2008).

However, since shallow loess landslides often occur on saturated, or nearly saturated, steep slopes and transfer into loess
flow, models such as the TRIGRS, which is based on the infinite slope model and is focused on forecasting shallow landslides
in areas with a gentle slope, are difficult to apply (Wang et al., 2015; Zhuang et al., 2017). SINMAP and SHALAD are
prediction models also based on infinite slope models and the sliding or soil depths are fixed parameters related to landforms
80 (Montgomery and Dietrich, 1994; Pack et al., 1999; Michel et al., 2020). According to previous studies, shallow loess
landslides with sliding-flow landslide characteristics are mainly induced by prolonged heavy rainfall and the sliding surface is
the saturated or nearly saturated layer (Wang and Sassa, 2001; Zhang et al., 2013; Peng et al., 2015; Wang et al., 2015; Zhuang
et al., 2017; Guo et al., 2019). Due to their small scale and difficult identification, shallow landslides on the CLP are a
significant safety threat to local residential areas (Peng et al., 2015; Wang et al., 2015; Guo et al., 2019; Zhang et al., 2020).
85 As most shallow loess landslides occur within the top 2 m and transfer into loess flow with high speed and a long runout, the
depth of the saturated layer is a critical factor when studying loess sliding-flow landslides induced by prolonged heavy rainfall.
However, there is no quantitative evaluation for the critical slip depth and, thus, it is not possible to construct a rainfall
criticality model based on physical processes.

The current study comprehensively evaluates the unique characteristics of shallow loess sliding-flow landslides triggered
90 by prolonged precipitation. Upon correcting for the safety factor being invariable or increasing with the increasing slope greater
than 40°, calculated using the Taylor slope infinite model via the equal differential unit method, the revised infinite slope
(RISM) model was proposed. The objectives of this study were to determine the sliding depths of the saturated layer at different
slopes, and, to consider rainfall intensity and duration for developing a shallow loess landslide prediction model using loess
infiltration characteristics. The model was verified using the 2013 “7.25” Tianshui sliding-flow landslide events in Tianshui
95 Gansu province, a sliding-flow loess landslide triggered by prolonged precipitation.

2 Study area

2.1 Geological and geomorphological

The study area is a hilly loess region located southwest of the CLP and is part of the transition zone between the Qinling Mountains and the Longshan Mountains (Peng et al., 2015; Zhang et al., 2020). The loess is deeply and widely distributed with vertical joints and fissures, creating a fragile geological environment where geohazards such as landslides and debris flows frequently occur (Peng et al., 2015; Zhang et al., 2020; Qi et al., 2021). The terrain of the study area is generally high in the southeast and low in the northwest, with altitudes ranging from 748.5 to 2,120 m and a relative height difference of 100 to 1,430 m. This geomorphic unit includes the loess hill area comprised of platforms (Yuan in Chinese), ridges (Liang in Chinese), domes (Mao in Chinese), and valleys. The loess hill area is divided by the Wei River and Western Han Rivers their tributaries, with thousands of ravines (Fig. 1). The tops of the loess hills are essentially horizontal surfaces at an altitude from 1,900 to 2,000 m and the relative height difference between the ridges is about 500 m. The Weihe River through the loess hilly area from west to east.

Tianshui City is located in the west wing of the Qilu-Helan Mountain zigzag structural system and the Qinling zonal structural belt. The sub-north-east-trending structural belts and Longxi structural insertions, folds, and compressive faults are highly developed in this area. The neotectonic movement is strong and the average annual elevation of the mountains is 0.6-8 mm. Additionally, the study area is located within the North-South and Tianshui-Lanzhou seismic belts, with frequent seismic activity (Sun et al., 2017).

2.2 Climate characteristics

The study area is a mid-latitude inland region and has a cold temperate semi-arid continental monsoon climate with four distinct seasons, dry winters, and springs (low precipitation) and hot and humid summers (high precipitation). The annual average temperature is 10.6 °C and the annual precipitation ranges from 400 to 700 mm.

Elevation is the primary factor affecting the precipitation amount, with high precipitation in the high-altitude area and low precipitation in the low-altitude area. The average annual rainfall is more than 700 mm in the study area. The rainfall in the region is typically moderate, accounting for 91% of the annual rainfall. According to the precipitation data in recent decades years (Peng et al., 2015; Zhang et al., 2020), the greatest precipitation occurred in 1967 with 772.2 mm and the least precipitation occurred in 1939 with 316.6 mm. There are also fluctuations in the annual rainfall distribution. Most rainfall is observed from June to September, representing 70% of the annual precipitation; 38% occurs in July and August (Peng et al., 2015; Zhang et al., 2020). In autumn 3013, long-duration and large-scale heavy rainfall resulted in severe flooding and geological disasters.

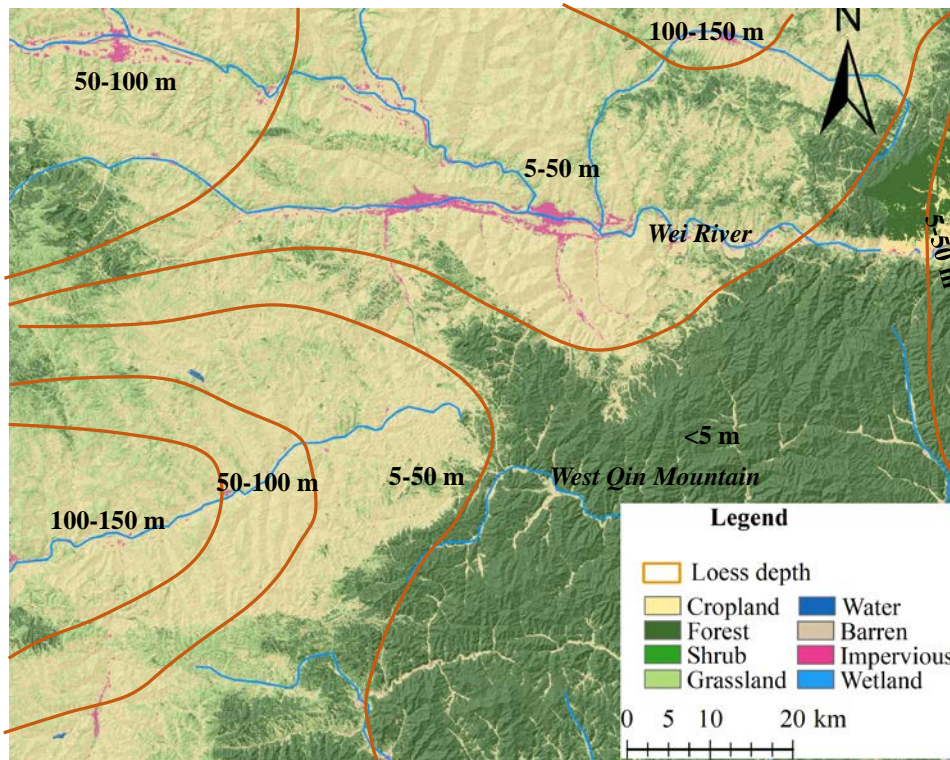


Figure 1. The geological and land use of the study area. Base DEM data from <https://geocloud.cgs.gov.cn/#/home>, land use data from <http://www.geodata.cn>.

Beginning on June 19, 2013, prolonged heavy precipitation occurred in the Tianshui region. The total cumulative precipitation and the maximum rainfall intensity of this event represent a 100-year return period (Peng et al., 2015; Qi et al., 2021). This heavy rainfall event lasted for 37 days and induced a mass sliding-flow landslide disaster. During this extreme rainfall event, there were four heavy rainfall stages, with different rainfall periods. The first heavy rainfall period began on June 19 at 19:00 and ended on June 21 at 4:00, with a cumulative rainfall of 285 mm, then from 3:00 to 20:00 on July 8 (128.9mm), followed by 16:00 on July 21 to 4:00 on July 22 (43.5mm), and the last period was from 23:00 on July 24 to 10:00 on July 25 (174.4mm) (Table 1). Over 45,000 shallow sliding-flow landslides were triggered, characterized by shallow and small scar areas, resulting in the death of 25 people.

Table 1. The precipitation data from the “7.25” Tianshui sliding-flow landslide events.

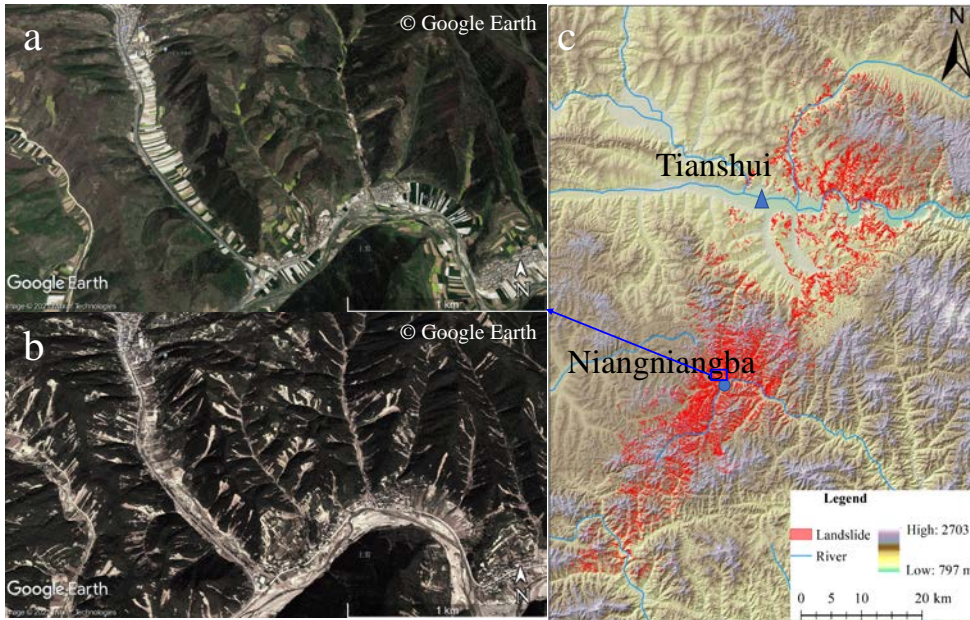
Date	Accumulative rainfall / mm	Duration / h	Average intensity / mm/h	Max intensity/ mm/h
19:00 on June 19 to 4:00 on June 21	285	34	8.382353	35.8
3:00 to 20:00 on July 8	128.9	17	7.582353	22.6
16:00 on July 21 to 4:00 on July 22	43.5	12	3.625	19
23:00 on July 24 to 10:00 on July 25	174.4	11	15.85455	32.2

设置了格式: 字体颜色: 自动设置

3 The “7.25” Tianshui sliding-flow landslide events characters

3.1 Landslide data

140 High-precision remote sensing imaging data (~2 m resolution from Google earth images) from October 2012 (before the sliding-flow landslide event) and December 2013 (after the sliding-flow landslide event), along with field observations, was used to determine that a total of 47,005 sliding-flow landslides occurred in the study area. It can be seen from Figure 2 that the sliding-flow landslide distribution is primarily concentrated in the middle of the study area along the NNE direction and decreased gradually to the southeast and northwest.



145 **Figure 2** The landslides triggered by “7.25” Tianshui sliding-flow landslide events (a: before “7.25” Tianshui sliding-flow landslide events in October 2012; b: after “7.25” Tianshui sliding-flow landslide events in December 2013; c: the landslides distribution triggered by “7.25” Tianshui sliding-flow landslide events; [Base DEM data from https://geocloud.cgs.gov.cn/#/home](https://geocloud.cgs.gov.cn/#/home))

150 The landslides occurred in the shallow loess layer at a depth of no more than 2 m and with sliding-flow landslide characteristics observed via a large number of field investigations. Normally, shallow landslides are triggered during prolonged heavy rainfall events by the rapid increase of pore pressure or loss of cohesion (Iverson 2000; Wang and Sassa 2001; Sassa and Wang 2005; Tu et al., 2009; Zhang et al., 2013). As a result, a failure surface develops within the soil profile or at the depth of the precipitation infiltration. This means that the sliding soil layer is close to liquid limit water content when the landslide starts, and flowing characteristics occur after the slope failure.

155 3.2 Size characters

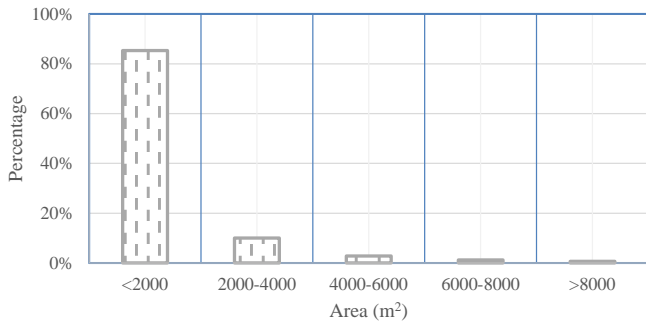
The sliding-flow landslide impacted area is 65.69 km² and the density is greater than 25 sliding-flow landslides per/km². As shown in Fig. 2, the area of sliding-flow landslides in Tianshui Niangniangba accounts for more than 35% of the total area, and shallow flow slips occurred on most of the slopes. The mean sliding-flow landslide area was 0.0013 km², which is smaller

160 than what is typical for landslides triggered by rainfall or earthquakes (Table 2). Fig. 3 shows the proportion of landslides in different areas. It can be seen that most of the sliding-flow landslides were smaller than 2,000 m² and accounted for more than 80% of the total landslides. Landslides larger than 5,000 m² accounted for only 3% (Fig. 3), indicating that the “7.25” Tianshui sliding-flow landslide events were primarily small sliding-flow landslides occurring in groups.

Table 2. Landslide size and numbers triggered by earthquakes or rainfall in recent years.

Items	Study area (km ²)	Number of landslide (km ²)	Landslide surface areas (km ²)	Average surface area of the landslide (per km ²)
Northridge earthquake (Harp and Jibson, 1996)	10,000	11,111	23.8	0.00214
Haiyuan Earthquake (Zhuang et al., 2018)	40,000	3,700	117.45	0.03162
Wenchuan Earthquake (Dai et al., 2011)	41,750	56,000	811	0.01448
Chi-Chi earthquake (Lin and Tung, 2004)	--	9,297	128	0.01374
Kashmir earthquake (Owen et al., 2008)	7,500	2,424	--	--
Umbria, Central Italy[rapid snowmelt] (Guzzetti et al., 2002)	2,000	4,233	12.7	0.00301
Guatemala [heavy rainfall] (Bucknam et al., 2001)	10,000	9,594	29.5	0.00307
“7.25” Tianshui sliding- flow landslide events	1,936	47,005	65.69	0.0013

设置了格式: 字体颜色: 自动设置



165 **Figure 3.** The proportion of “7.25” Tianshui sliding-flow landslides in different areas.

Fig. 4 depicts the “7.25” Tianshui sliding-flow landslide area, cumulative frequency distribution, and statistical significance of sliding-flow landslides with an area of failure $\geq 5,000 \text{ m}^2$, accounting for 90% of the total landslides. The largest landslide was only 0.099 km^2 . We examined the area-frequency distribution of the “7.25” Tianshui sliding-flow landslide events via log-binning a normalized non-cumulative size-frequency distribution to plot frequency-density ($\text{Lg}N = aA + b$, where N refers to the number of landslides in each bin) as a function of binned landslide area (A) (Fig.4) (Stark and Hovius, 2001; Malamud et al., 2004;). The higher value a may reflect a greater ability to identify smaller landslides via high-quality imagery. The value for the “7.25” Tianshui sliding-flow landslide events ($a = -2.83$) is higher than the exponents reported for other coseismic inventories. For example, $a = -2.39$ for Northridge, California, $a = -2.30$ for Chi Chi, Taiwan, $a = -2.19$ for Wenchuan, China, and $a = -2.3$ for the average of event-based and historical inventories reported by Van den Eeckhaut et al. (2007) (Roback et al., 2018), also showing that landslides triggered by the “7.25” Tianshui sliding-flow landslides were primarily small landslides occurring in groups.

175

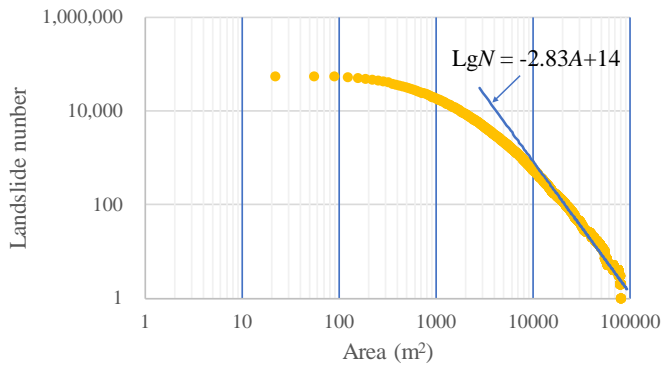
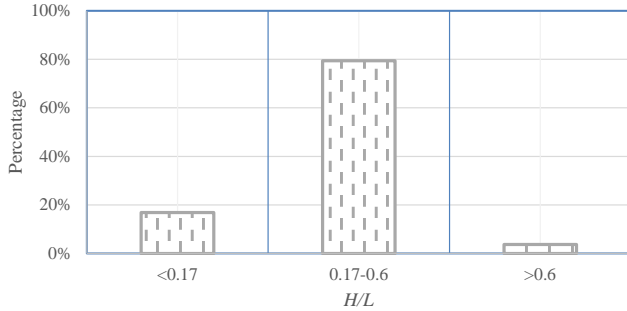


Figure 4. The cumulative frequency distribution of “7.25” Tianshui sliding-flow landslide area.

180 **3.3 Mobility characteristics**

We examined the probability densities of equivalent friction coefficients (landslide vertical height (H) / landslide travel distance (L)) for the “7.25” Tianshui sliding-flow landslide events using Matlab (Fig. 5). The landslide vertical height (H) was based on the altitudes of the highest and the lowest points, and the movement distance was the distance between the highest point and the lowest point. The above two parameters were obtained and calculated using ArcGIS spatial analysis.

185 The H/L ratio frequency ratio of the “7.25” Tianshui sliding-flow landslide events, ranged from 0.01 to 0.88 with a mean of 0.32. According to a study by Wang (2000), landslide fluidization occurs when the equivalent friction coefficient is below 0.17. In our study, 16.85% of the loess sliding-flow landslides had equivalent friction coefficients below 0.17, indicating that the loess sliding-flow landslides moved with flow motion and resulted in longer sliding distances. For more than 96.27% of landslides, H/L was less than 0.6 ($H/L < 0.6$ indicates a long-runout landslide) and belongs to long run-out landslides.

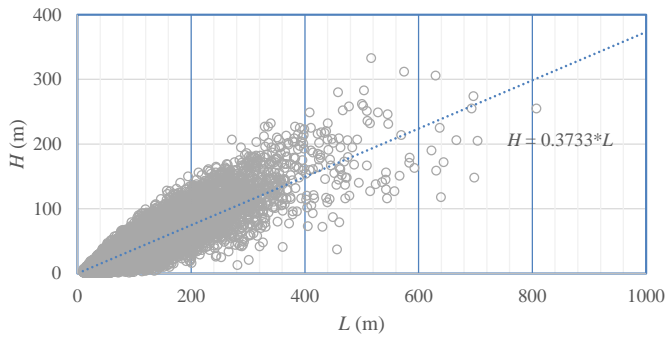


190

Figure 5. The probability densities of equivalent coefficients of friction of “7.25” Tianshui sliding-flow landslides.

To model the empirical relationship between sliding-flow landslide height and travel length, which was later verified using images and field investigations, the aforementioned datasets were analyzed to plot H and L on a single graph (Fig. 6), where L (x-axis) is the landslide travel distance and H (y-axis) is the landslide height.

195 The relationship between height difference and travel distance is positively correlated. With an increase in the height differential, the travel distance increased and the slope of the fitting trend line between the height difference and travel distance was 0.37, indicating that the travel distance is greater than the height difference and shows evident long-runout travel distance characteristics.

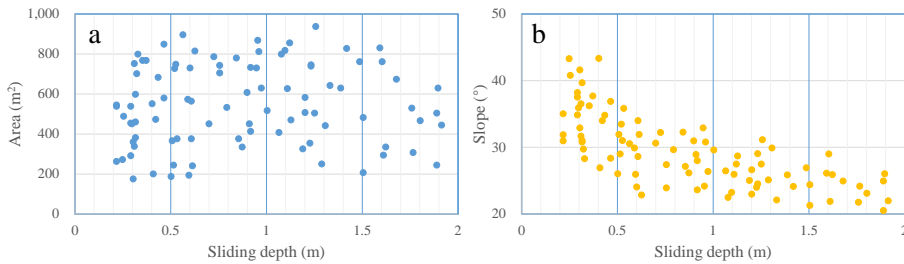


200 **Figure 6.** The relationship between height differential and travel distance of the “7.25” Tianshui sliding-flow landslides.

3.4 Sliding depth characteristics

To obtain sliding-flow landslide depths, we conducted a detailed investigation of sites throughout the study area, such as Niangniangba town, and obtained depth data for 83 landslides based on the characteristics of the sliding-flow landslide and the thickness of the loess scar at the edge of the landslide. Fig. 7 displays the distribution of sliding-flow landslide depths and area; no landslide had a depth greater than 2.0 m and over 70% ranged from 0 to 1 m (Fig. 7). Additionally, we found that the depth of the sliding-flow landslide had no correlation with the landslide area and had a negative correlation with the slope. With increasing slope, the depth of the landslide decreases, that is, the greater the slope, the shallower the sliding surface, and the smaller the slope, the greater the depth of the sliding surface.

205



210

Figure 7. The distribution of sliding-flow landslide depths and area of the “7.25” Tianshui sliding-flow landslides, a) landslide surface area vs sliding surface depth and b) slope vs sliding surface depth.

At the meanwhile, the slope and sliding-flows landslides distribution in the study area were statistic, and it can be seen that most sliding-flows landslides had a gradient value with in the range of 30–50°, while landscape areas were concentrated in the range of 10–30°. And, the sliding-flows landslides with slopes greater than 50° accounted for 13.81% in the study area. As a result, the failure probability of sliding-flow landslides can occurred on steep slopes (50°) in the Loess Plateau region.

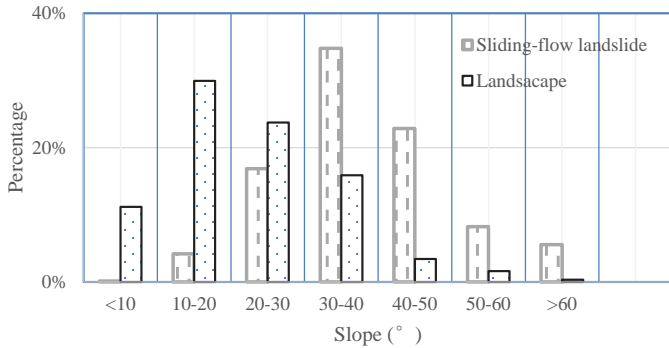


Figure 8. Map showing the relationship between the sliding-flows landslide, landscape, and slope.

3.5 The shallow sliding-flow landslide formation process

Force analysis shows that a slope will fail when the gravity component along the slope direction is greater than the shear strength of the soil (Sassa, 2000; Ochiai et al., 2004; Gabet and Mudd, 2006). If the stability coefficient of the slope is high and the soil reaches its liquid limit water content before the failure, the slope will spontaneously liquefy and flow during the sliding process (Wang and Sassa, 2001; Wang et al., 2015). Usually, the ratio of pore-water pressure to the total normal stress of the soil is used to express the soil liquefaction ratio. When the liquefaction rate is 1, the pore-water pressure equals the normal stress of the soil and the failing slope is in a state of complete liquefaction (Hung et al., 2001; Wang and Sassa, 2001; Sassa and Wang, 2005; Wang et al., 2015). Typically, the normal stress of shallow landslides is low and the slope deformation is attributed to decreased strength. The soil has an obvious volume reduction due to the large pore structure of the collapsing soil structure, followed by a sharp increase in the pore-water pressure (Wang and Sassa, 2001; Sassa and Wang, 2005; Peng et al., 2018). Shallow sliding-flow landslides are triggered by prolonged heavy precipitation and rainfall infiltration to a certain loess depth (mostly 1-2m) close to liquid limit water content, followed by a decrease in the soil strength (Tu et al. 2009; Xu et al., 2011; Zhuang et al. 2018). When the anti-slip force of the saturated soil is less than the sliding force, the saturated soil layer will fail. Due to the large pore structure of the soil, once soil deformation occurs, the water in the pores cannot be released, resulting in the pore-water pressure increasing sharply which causes liquefaction of the saturated soil to form a mudflow (Fig. 89).

设置了格式: 字体颜色: 自动设置
 带格式的: 行距: 1.5 倍行距, 孤行控制
 设置了格式: 字体颜色: 自动设置
 设置了格式: 字体颜色: 自动设置
 设置了格式: 字体颜色: 自动设置
 设置了格式: 字体颜色: 自动设置
 设置了格式: 字体颜色: 自动设置

设置了格式: 字体: (默认) Times New Roman, (中文) Times New Roman, 10 磅, 加粗, 英语(英国)
 设置了格式: 字体: (默认) Times New Roman, (中文) Times New Roman, 10 磅, 英语(英国)
 设置了格式: 字体颜色: 自动设置
 设置了格式: 字体: (默认) Times New Roman, (中文) Times New Roman, 英语(英国)
 设置了格式: 字体: (默认) Times New Roman, (中文) Times New Roman, 10 磅, 英语(英国)
 设置了格式: 字体: (默认) Times New Roman, (中文) Times New Roman, 10 磅, 英语(英国)

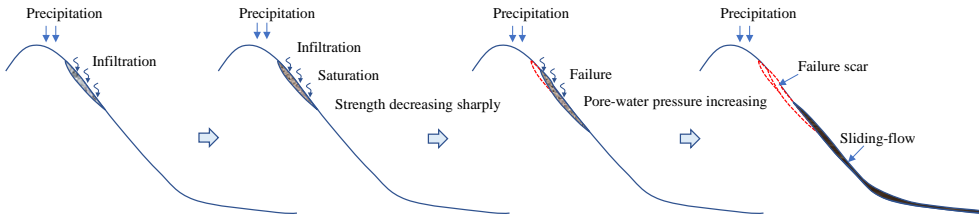


Figure 89. The shallow sliding-flow landslide formation process.

4 Forecast model of shallow loess landslide development

4.1 Infinite Slope Model

According to field investigations and other research results, the shallow sliding-flow landslides are concentrated within 2 m of the surface and are negatively correlated with slope (Tu et al. 2009; Xu et al., 2011; Zhuang et al., 2017; Zhuang et al. 2018; Zhuang et al., 2022). Therefore, infinite slope models considering the thickness of the soil layer and the maximum infiltration depth cannot be directly applied in shallow landslide assessments. Previous studies have shown that short-duration heavy precipitation has less impact on the stability of loess slopes, whereas, prolonged heavy precipitation increases the water content significantly and reduces the slope stability (Wang and Sassa, 2001; Wang et al., 2015; Peng et al., 2018). Shallow landslides transformation to mudflows occurs most often on slopes of 25 to 45°, and the sliding body is close to the liquid limit water content before slope instability. Pore-water pressure is a key factor for soil slope failure (Iverson 2000). Previous studies have shown that pore water pressure is the cause of soil landslides, and excess pore-water pressure is the triggering factor for its fluidization (Iverson et al., 1997; Sassa and Wang 2005; Gabet and Mudd, 2006). Failure of the sliding body is primarily due to a decrease in soil strength which results in the sliding force being greater than the cohesive forces following rainfall infiltration which saturates the soil (Wang et al., 2015; Peng et al., 2018).

According to the infinite slope model (Fig. 910), Taylor proposed the following safety factor equation (Taylor, 1948):

$$K = \frac{(\gamma_{sat} - \gamma_w)h_w \cos^2 \alpha \tan \phi' + c'}{\gamma_{sat} h_w \sin \alpha \cos \alpha}, \quad (1)$$

where α is the slope angle, γ_w is the soil floating weight, γ_{sat} is the saturation weight of the soil, b is the length of the sliding body, h_w is the depth of the sliding surface, and the approximate depth of loess at the liquid limit water content due to infiltration, c' (cohesive), and ϕ' (internal friction angle) is the effective strength index of the soil at the sliding surface.

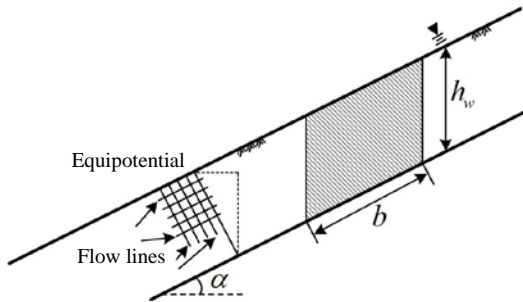


Figure 9-10 The cross-section of an infinite slope (Modified from Taylor, 1948).

Using the mean strength of the saturated loess, the stability factor is calculated according to the infinite slope model proposed by Taylor (Taylor, 1948). The results are shown in Fig. 4011.

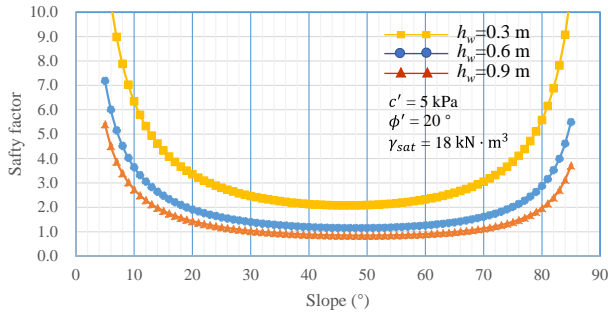


Figure 4011. The safety factor according to the infinite slope model proposed by Taylor.

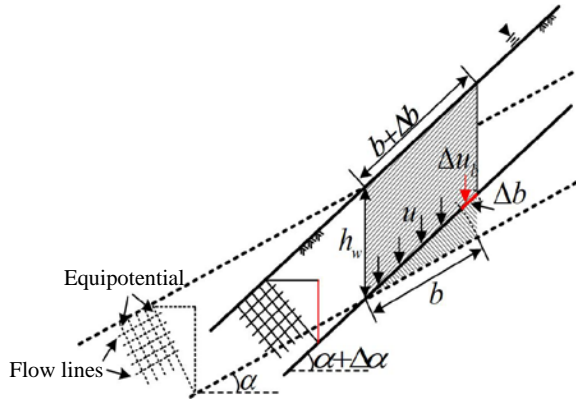
Figure 40-11 shows that for a cohesive soil slope, the safety factor decreases with increasing slope when the slope is less than 40°. There is little difference for slope from 40 to 50°; however, the safety factor increases when the slope is great than 50°. The calculated results are inconsistent with the actual situation, in particular, the model shows the safety factor increases with increasing slope—which is incorrect. However, almost all shallow landslide physical prediction models (eg: TRIGRS, SINMAP, SHALAD) are based on the infinite slope model proposed by Taylor, so these shallow landslide physical prediction models cannot be applied to areas of high slope (>40°), reducing wide use of these models (Montgomery and Dietrich, 1994; Baum et al., 2008; Zhuang et al., 2017).

4.2 Revised Infinite Slope Model

270 To make the calculation results of Taylor's infinite slope model conform to the actual situation, this study modified the Taylor infinite slope model using an equal differential unit method. As shown in Fig. 4-12, by keeping the depth of the saturation zone unchanged with increasing slope, the formula for calculating the self-weight of the soil strip unit can be revised as:

$$W = \gamma_{sat} h_w (b + \Delta b) \cos(\alpha + \Delta\alpha), \quad (2)$$

Where b is the length of the sliding body and $\Delta\alpha$ is the value of the increasing slope.



275 **Figure 4-12.** Figures demonstrating the infinite slope model with variation in slope.

In Eq. (2), the self-weight of the soil strip unit and the control condition of the soil strip area are unchanged:

$$h_w (b + \Delta b) \cos(\alpha + \Delta\alpha) = h_w b \cos \alpha, \quad (3)$$

280 Eq. (2) shows that, although the change of slope does not affect the self-weight of the differential element, it leads to a change in the bottom area of the element, which causes the cohesion strength and pore water pressure of the bottom surface of the soil strip element to change. The change of the slope only affects the component values of the forces in the normal and tangential directions of the sliding surface. Therefore, it is necessary to remove the changes in cohesion strength and pore water pressure caused by increasing the slope of $\Delta\alpha$ when calculating the slope stability with different slopes.

285 The change in cohesive strength (ΔC) and pore water pressure (Δu_b) resulting from increasing the slope of $\Delta\alpha$ are described as:

$$\Delta C = c' \Delta b, \quad (4)$$

$$\Delta u_b = \gamma_w h_w \Delta b \cos^2(\alpha + \Delta\alpha), \quad (5)$$

The effective normal stress (N') and effective anti-sliding force (T_f) at the bottom of the soil strip element due to the slope increasing from α to $\alpha + \Delta\alpha$ is expressed as:

$$290 \quad N' = \gamma_{sat} h_w (b + \Delta b) \cos^2(\alpha + \Delta\alpha) - \gamma_w h_w (b + \Delta b) \cos^2(\alpha + \Delta\alpha), \quad (6)$$

$$T_f = [\gamma_{sat} h_w (b + \Delta b) \cos^2(\alpha + \Delta\alpha) - \gamma_w h_w (b + \Delta b) \cos^2(\alpha + \Delta\alpha)] \tan \phi' + c' (b + \Delta b), \quad (7)$$

The sliding force of the soil strip unit is changed to:

$$S = \gamma_{sat} h_w (b + \Delta b) \cos(\alpha + \Delta\alpha) \sin(\alpha + \Delta\alpha), \quad (8)$$

The revised effective anti-slip force according to the Eqs. (4), (5), and (7) is:

$$T_f = [\gamma_{sat} h_w (b + \Delta b) \cos^2(\alpha + \Delta\alpha) - \gamma_w h_w b \cos^2(\alpha + \Delta\alpha)] \tan \phi' + c' b, \quad (9)$$

Combining Eqs. (8) and (9), the safety factor can be obtained:

$$K = \frac{[\gamma_{sat} \cos \alpha - \gamma_w \cos(\alpha + \Delta\alpha)] h_w \cos(\alpha + \Delta\alpha) \tan \phi' + c'}{\gamma_{sat} h_w \cos \alpha \sin(\alpha + \Delta\alpha)}, \quad (10)$$

Making $\alpha = \alpha_1$, $\alpha + \Delta\alpha = \alpha_2$, $(\alpha_1, \alpha_2) \in \alpha$, Eq. 10 can be expressed as:

$$K = \frac{(\gamma_{sat} - \gamma_w m_\alpha) h_w \cos \alpha_2 \tan \phi' + c' \sec \alpha_1}{\gamma_{sat} h_w \sin \alpha_2}, \quad (11)$$

305 Making $m_\alpha = \frac{\cos \alpha_2}{\cos \alpha_1}$, for the simple equation, the term $c' \sec \alpha_1$ in Eq. (11) can be defined as the reference cohesion strength.

Since the value of $c' \sec \alpha_1$ varies monotonically with α_1 changing, to make the reference cohesion strength corresponding to any slope angle equal, it only needs to satisfy that α_1 is less than or equal to α_2 :

$$\alpha_1 = \min\{\alpha_2\}, \alpha_2 \in \alpha. \quad (12)$$

Therefore, the safety factor of the RISM can be expressed as:

$$310 K = \frac{(\gamma_{sat} - \gamma_w \cos \alpha) h_w \cos \alpha \tan \phi' + c'}{\gamma_{sat} h_w \sin \alpha}, \quad (12)$$

Using the mean strength of saturated loess in the loess area, the stability is calculated according to the RISM proposed by this study, and the results are shown in Fig. 4213. The RISM according to the using equal differential unit method corrects the safety factor that increases with the slope increasing when the slope is larger than 50° (calculated using the Taylor slope infinite model). The results obtained by the RISM maintain consistency with the calculation result of the Taylor method at low angles, and the calculated results decrease with an increased slope when the slope is larger than 40°.

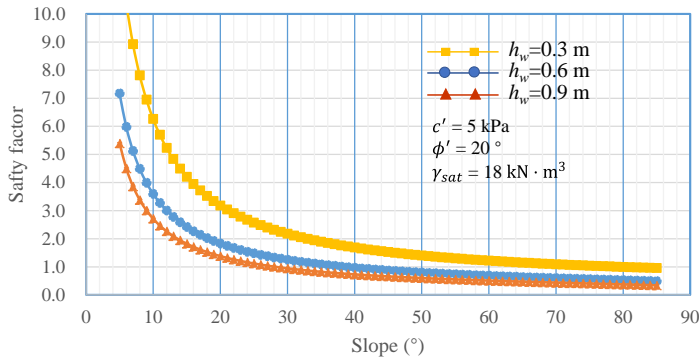


Figure 1213. The safety factor according to the RISM.

4.3 Critical depth of shallow loess landslides

When the stability coefficient K is 1 in Eq. (12), the critical depth of loess close to liquid limit water content, or the sliding surface of the shallow loess landslide, can be obtained:

$$h_{cr} = \frac{c'}{\gamma_{sat} \sin \alpha - (\gamma_{sat} - \gamma_w \cos \alpha) \cos \alpha \tan \phi'}, \quad (13)$$

The critical liquid limit water content depth, or the sliding surface of the shallow loess landslide, for different slopes can be determined by obtaining the soil strength of the nearly saturated state. When the liquid limit water content reaches the critical depth, the layer will fail. The cohesion and angle of internal friction were tested using the triaxial test method at saturation following the soil test standard GBT50123-1999. According to the loess test results, the cohesive forces of undisturbed loess at the liquid limit water content (0-2 m) range from 3 to 9 kPa with an average of 5 kPa, and the internal friction angle ranges from 11 to 21° with an average of 15° (Fig. 1314). Therefore, the relationship between the critical approximate liquid limit water content depth and the slope can be calculated. With increasing slope, the critical approximate liquid limit water content layer gradually decreases, but the rate of decrease slows, from 1.14 m at 20° to 0.47 m at 40° (Fig.

1314). This relationship can be expressed via the power-law as:

$$h_w = 34.13a^{-1.15}, \quad (14)$$

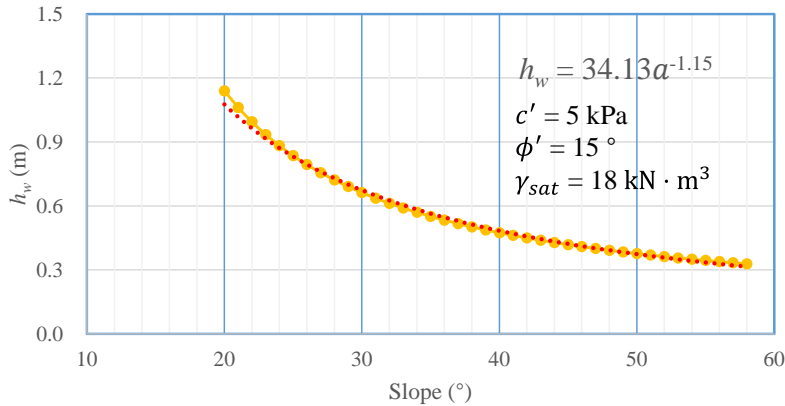


Figure 1314. The relationship between the critical depth and the slope.

设置了格式: 字体颜色: 自动设置

4.4 The I-D curve of the loess shallow landslide

330 The critical rainfall intensity-duration (*I-D*) method is often used in forecasting rainfall-induced shallow landslides (Guzzetti et al., 2007; Guzzetti et al., 2008; Baum and Godt, 2010; Zhuang et al., 2015). Thresholds empirically derived from rainfall intensity-duration have been widely used to identify rainfall conditions that result in the occurrence of landslides (Guzzetti et al. 2007; Guzzetti et al. 2008; Baum and Godt 2010). Inspection of the *I-D* thresholds reveals the general form:

$$I = \beta D^b + c, \quad (6)$$

335 Where *I* is the mean rainfall intensity, *D* is rainfall duration, and *c*, β , and *b* are other parameters. For the majority of *I-D* thresholds, *c* = 0, and Eq. 6 takes the form of a simple power law.

$$I = \beta D^b, \quad (7)$$

Previous studies have created statistical *I-D* curves based on landslide data and rainfall data. However, these empirical models require many years of precipitation data and calibration parameters. Even so, the determination of the landslide threshold *I-D* curve is inaccurate due to the uncertainty of rainfall monitoring, such as the location, quantity of monitoring sites, and the definition of the start and end time of rainfall events (Zhuang et al., 2015; Guo et al., 2016).

340

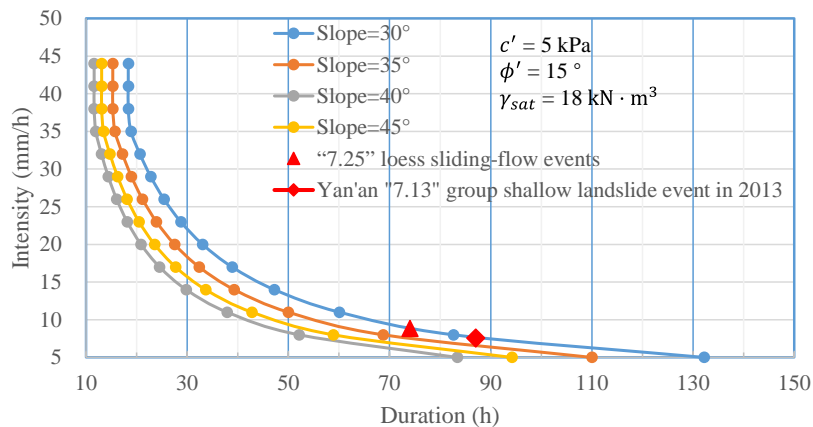
The critical *I-D* curve for slope instability for different slopes can be constructed using the critical approximate liquid limit water content depth model combined with the saturated infiltration characteristics of loess in the study area. Six infiltration tests were carried out in the study area using the single-ring infiltration test to determine the infiltration coefficient

345 (*i*) of loess under rainfall. The constant infiltration rates were: 38.6, 33.1, 39.1, 32.2, 36.2, and 31.6 mm/h. Additionally, it was observed that the time between initial infiltration and stable infiltration is less than 10 min. Therefore, in this study, the average stable infiltration rate of 36.0 mm/h was selected as the infiltration coefficient.

$$D = h_w / i, \quad \text{for the precipitation intensity is higher than the infiltration coefficient} \quad (8)$$

350 $D = h_w / I, \quad \text{for the precipitation intensity is lower than the infiltration coefficient} \quad (9)$

To model the relationship between *I* and *D*, the two variables were plotted on a single graph, where *D* (x-axis) is the rainfall duration and *I* (y-axis) is the rainfall intensity. According to the critical sliding surface depth under different slopes (Eq. 14), curves *I* and *D* under different slopes can be calculated by using eq. 7 and 8. The *I-D* curve of the different slopes in the area can be obtained based on the infiltration coefficient and the sliding depth (Fig. 14-15).



355

Figure 14: The *I-D* curve of the different slopes in the loess area.

5 Discussion

5.1 Model compare

360 Comparing the *I-D* curves for different slopes with the existing models, it was found that *I-D* curves constructed based on the physical model in this study are higher than for other models which are statistical lines and a probabilistic model. Meanwhile, the *I-D* curves of other areas are obtained through statistics, and even though a single landslide occurs in this area, it will be counted as a landslide event. Meanwhile, many researchers have pointed out that antecedent rainfall plays a significant role in triggering landslides in loess areas which is different for other regions, such as Hong Kong, fire impacted areas in the US, and the southwest mountains in China (Cui et al., 2008; Zhuang et al., 2015). Therefore, the *I-D* curves of other areas will be lower than the *I-D* curve constructed based on physical models (Fig. 15:16).

365

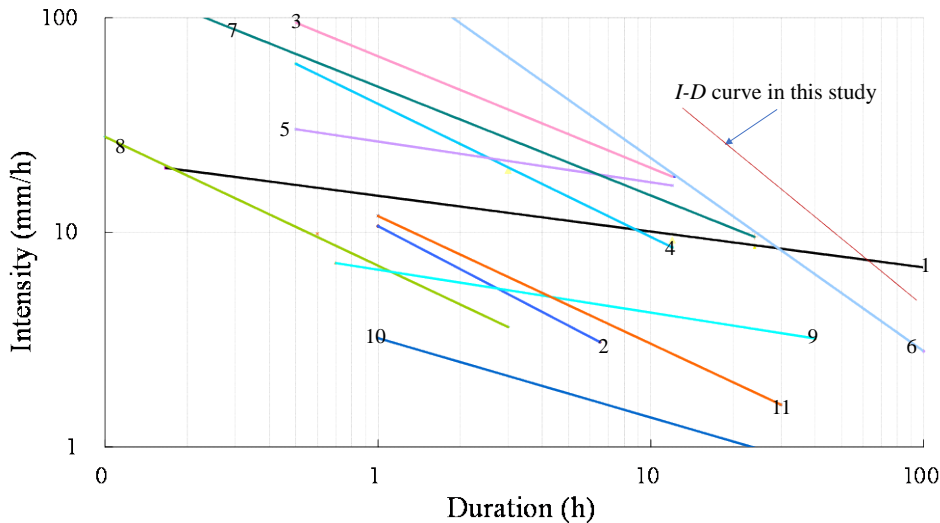


Figure 4516. Comparison of I-D curves from the current and prior studies (No.1: Caine 1980; No. 2: Wieczorek 1987; No. 3, 4, 5: Jibson 1989; No. 6: Guadagno 1991; No. 7: Paronuzzi et al. 1998; No. 8: Crosta and Fratini 2001; No. 9: Shieh et al. 2009; No. 10: Guo et al. 2013; No. 11: Zhuang et al., 2015).

From the distribution of shallow landslides in this area, it can be seen that the shallow landslides in this area mainly occur on slopes of 35 to 50°. Marking the rainfall duration and intensity of the “7.25” Tianshui sliding-flow landslide events and the “7.13” group shallow landslide in Yan’an in 2013 (Wang et al., 2015; Zhuang et al., 2017) on the *I-D* line, it can be seen that the rainfall duration and intensity of both events are above the *I-D* curve of 35°, indicating that the constructed curve is reliable and can be used to forecast shallow landslides in this area.

5.2 Model limitations

Previous studies have assumed that restoration of vegetation is beneficial for preventing landslides, mainly because of the reinforcement effect of roots on soil (Waldron, 1977; Roering et al., 2003). However, the inhibitory effect of vegetation on landslides is gradually being questioned due to research on the negative relationship between vegetation and landslides in recent mass landslides in loess and other well-vegetated areas. For example, the “9.16” mass shallow landslides in Changning, Yunnan in 2014, the Yan’an “7.13” mass shallow landslides event, the 2015 Tianshui mass shallow landslides event, and the 2010 Nanping mass shallow landslides event in Fujian Province all had mass shallow landslides induced by prolonged heavy precipitation, often occurring in areas well-vegetated areas (Fig. 4617, Wang et al., 2015; Peng et al., 2015; Zhuang et al.,

带格式的: 两端对齐, 定义网格后自动调整右缩进, 行距: 1.5 倍行距, 孤行控制, 调整中文与西文文字的间距, 调整中文与数字的间距

设置了格式: 字体颜色: 自动设置

设置了格式: 字体颜色: 自动设置

2017; Zhang et al., 2020). Due to the complexity of the influence of vegetation on slope stability, most of the studies have not clarified whether the vegetation induces or inhibits landslides (Rickli and Graf, 2009; Preti, 2013; Zhuang et al., 2022). In general, plant roots can reinforce the slope soil and improve the shear strength of the soil (Waldron, 1977; Roering et al., 2003). However, the increase of vegetation can also result in greater stored precipitation and infiltration into the soil (Wang et al., 2015; Zhuang et al., 2017; Zhuang et al., 2022). Plant root systems also provide channels for preferential flow, resulting in greater soil water contents which promote the occurrence of landslides (Zhuang et al., 2017; Zhuang et al., 2022). The vegetation on the Loess Plateau is often shrubs with shallow root systems that do not exceed the sliding surface. Since most shallow landslides slide along the bottom of the root system, according to field investigations, they do not prevent these landslides (Wang et al., 2015). Slopes with good vegetation coverage increase the weight of the sliding body during precipitation. The prediction model proposed in this study does not consider the impact of vegetation on shallow landslides. According to data from monitoring numerous loess areas, increased restoration of vegetation results in more rainwater infiltrating into the loess, increasing the water content of the shallow loess, and results in an increased possibility of shallow landslides. There is not only downward vertical infiltration but also horizontal infiltration along the slope direction in the process of rainfall infiltration on the slope surface resulting in the confluence of water in the slope body (Wang et al., 2015; Zhuang et al., 2022).

At the same time, according to the assumption of the infinite slope model, it is mainly applicable to the slope extent is much larger than the depth of potential slip surface, slope angle is not too large, and soil characteristics are homogeneous along the slope direction, which means that the infinite slope model is only suitable for homogeneous soil slope instability prediction due to rainfall-induced (Taylor, 1948).

For slopes constituted of binary structures slope and failure controlled by the strength of the structure of the rock-soil mass is often not able to evaluate a correct factor of safety for the slope. So the Revised Infinite Slope Model is also suitable for homogeneous soil slopes, and slope extent is undefined or much larger than the depth of potential slip surface, but can be applied to steeper slopes in Loess Plateau.

设置了格式: 字体颜色: 自动设置

设置了格式: 字体: (默认) Times New Roman, (中文) Times New Roman

设置了格式: 字体: (默认) Times New Roman, 字体颜色: 自动设置, 图案: 清除

设置了格式: 字体: (默认) Times New Roman, 字体颜色: 自动设置, 图案: 清除

设置了格式: 字体: (默认) Times New Roman, 字体颜色: 自动设置, 图案: 清除

设置了格式: 字体: (默认) Times New Roman, 字体颜色: 自动设置, 图案: 清除

设置了格式: 字体颜色: 自动设置

设置了格式: 字体: (默认) Times New Roman, 字体颜色: 自动设置, 图案: 清除

设置了格式: 字体: (默认) Times New Roman, 字体颜色: 自动设置, 图案: 清除

设置了格式: 字体: (默认) Times New Roman, 字体颜色: 自动设置, 图案: 清除

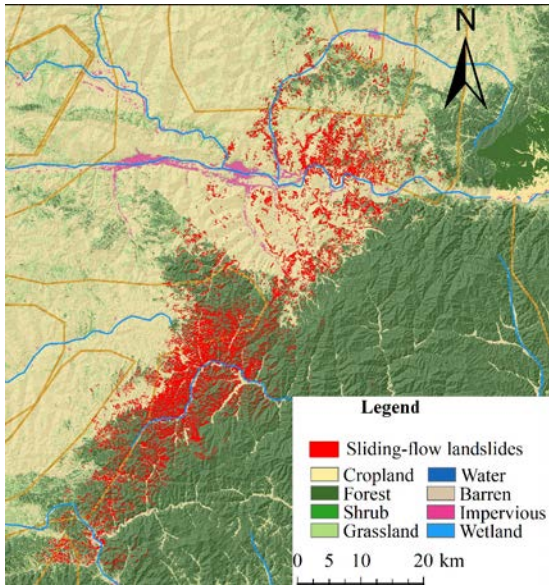


Figure 17. The “7.25” Tianshui sliding-flow landslides and land use in the study area (Base DEM data from <https://geocloud.cgs.gov.cn/#/home>, land use data from <http://www.geodata.cn>.)

5.3 Sensitivity analysis

410 Dry loess has high cohesive strength but loses strength significantly when wetted (Derbyshire et al. 2001; Zhuang et al., 2018) and has water-sensitivity characteristics, with the strength parameters changing rapidly with the water content increasing. According to existing research, the cohesion of loess can be reduced from greater than 50 kPa at a low water content to less than 10 kPa at high water content (Zhuang et al., 2018). The internal friction angle of loess varies slightly, generally from about 25° in low water content to about 16° in a saturated state. To assess the loess strength influence on shallow loess

415 landslides caused by prolonged heavy precipitation, the response of the slope stability to the strength change of saturated loess was calculated. Our results demonstrate that slope stability is greatly affected by cohesion, while the stability of the slope is less responsive to changes in the internal friction angle. Meanwhile, by changing the slope and fixing loess strength, the relationship between the safety factor and slope was obtained. The safety factor is varying obviously with slope changing, indicating that the cohesion and slope are key factors affecting soil stability and shallow landslides. Whereas the internal

420 friction angle has minimal effect on shallow landslides in loess areas (Fig. 4718).

带格式的: 缩进: 首行缩进: 0 字符

设置了格式: 字体: 加粗

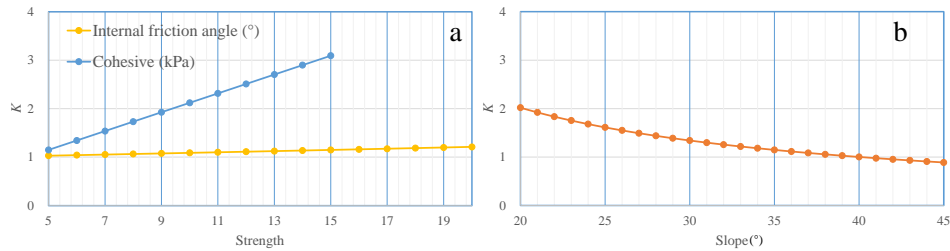


Figure 1718. The safety factor varies with internal friction angle, cohesion changing, and slope.

Conclusions

425 A rainfall-induced slope failure is a common cause of shallow landslides in the Loess Plateau. This study examines the shallow loess landslide triggered by prolonged heavy rainfall on July 25, 2013, in Tianshui, China, as a case study. The following results were obtained:

430 1. The “7.25” Tianshui sliding-flow landslide events triggered 47,005 landslides with a total area of 65.69 km² and the mean landslide area was 0.0013 km², which is smaller than most landslides triggered by other rainfall or earthquakes. Most of the landslides evaluated (80%) are smaller than 2,000 m² and landslides larger than 5,000 m² accounted for only 3%, indicating that the “7.25” Tianshui sliding-flow landslide events are primarily small landslides with group occurrences characters.

2. The *H/L* ratio frequency ratio of the “7.25” Tianshui sliding-flow landslide events, ranged from 0.01 to 0.88 with a mean of 0.32. The equivalent coefficient of friction was below 0.17 for 16.85% of the loess landslides, indicating that the loess landslide travels via flow motion, resulting in sliding longer distances.

435 3. The Revised Infinite Slope Model (RISM) was proposed using an equal differential unit method that corrects for any deficiencies associated with increased safety factors on slopes that are invariable or increasing when the slope is greater than 40° according to the Taylor slope infinite model.

440 (4) The critical approximate liquid limit water content depth (also the sliding surface depth) of the shallow loess landslides with different slopes can be described as $h_w = 34.13a^{-1.15}$. The critical *I-D* curve for slope instability for different slopes was constructed using the infiltration characteristics of loess in the study area.

Code and data availability. The data in this study were analysed with the Excel, and the figures were created with ArcViewTM GIS and Excel. All codes and date used in this work are available upon request.

445 *Author contributions.* Conceptualization, J. Z. and J. B.; methodology, J. Z. and C. H.; investigation, J. Z., J. B., J. X. and Y. Z.; data curation, J. Z. and J. X.; writing—original draft preparation, J. Z.; writing—review and editing, J. Z.; project administration, J. Z.; funding acquisition, J. Z. All authors have read and agreed to the published version of the manuscript.

Competing interests. The authors declare no conflict of interest.

Disclaimer. Publisher's note: Copernicus Publications remains neutral with regard to jurisdictional claims in published maps and institutional affiliations.

450 *Acknowledgements.* The authors are very grateful to the anonymous reviewers and editors for their thoughtful review comments and suggestions which have significantly improved this paper. This study was financially supported by the National Natural Science Foundation of China: 42090053, 41922054. The authors thank AiMi Academic Services (www.aimieditor.com) for the English language editing and review services.

设置了格式: 字体颜色: 自动设置

References

- Ahmadi-adli, M., Huvaj, N. and Toker, N.: Rainfall-triggered landslides in an unsaturated soil: a laboratory flume study, *Environ Earth Sci.*, 76, 735, doi:10.1007/s12665-017-7049-z, 2017.
- Baum, R.L. and Godt, J.E.: Early warning of rainfall-induced shallow landslides and debris flows in the USA, *Landslides*, 7, 259-272, doi:10.1007/s10346-010-0204-1, 2010.
- Baum, R.L., Savage, W.Z. and Godt, J.W.: TRIGRS-A FORTRAN program for transient rainfall infiltration and gridbased regional slope stability analysis, version 2.0. U.S. Geological Survey Open-File Report, 2008-1159, 75, 2008.
- 460 Berti, M., Bernard, M., Gregoretti, C. and Simoni, A.: Physical interpretation of rainfall thresholds for runoff-generated debris flows, *Journal of Geophysical Research: Earth Surface*, 125(6), e2019JF005513, doi:10.1029/2019JF005513, 2020.
- Bordoni, M., Galanti, Y., Bartelletti, C., Persichillo, M.G., Barsanti, M., Giannecchini, R., Avanzi, G.D., Cevasco, A., Brandolini, P., Galve, J.P. and Meisina, C.: The influence of the inventory on the determination of the rainfall-induced shallow landslides susceptibility using generalized additive models, *CATENA*, 193, 104630, doi:10.1016/j.catena.2020.104630, 2020.
- 465 Bordoni, M., Meisina, C., Valentino, R., Lu, N., Bittelli, M. and Chersich, S.: Hydrological factors affecting rainfall-induced shallow landslides: From the field monitoring to a simplified slope stability analysis, *Eng. Geol.*, 193, 19–37, doi:10.1016/j.enggeo.2015.04.006, 2015.
- Brenning, A.: Spatial prediction models for landslide hazards: review, comparison and evaluation, *Nat. Hazards Earth Syst. Sci.*, 5, 853-862, doi:10.5194/nhess-5-853-2005, 2005.
- 470 Bucknam, R.C., Coe, J.A., Chavarri'a, M. M., Godt, J.W., Tarr, A.C., Bradley, L.A., Rafferty, S., Hancock, D., Dart, R.L. and Johnson, M.L.: Landslides triggered by Hurricane Mitch in Guatemala—inventory and discussion, Open-File Rep. (U. S. Geol. Surv.), 2001–443, 38, doi:10.3133/ofr01443, 2001.

- Caine, N.: The rainfall intensity-duration control of shallow landslides and debris flows, *Geogr Ann (Series A: Physical Geography)*, 62, 23–27, doi: 10.1007/s10346-007-0112-1, 1980.
- 475 Cevasco, A., Brandolini, P., Scopesi, C. and Rellini, I.: Relationships between geo-hydrological processes induced by heavy rainfall and land-use: The case of 25 October 2011 in the Vernazza catchment (Cinque Terre, NW Italy), *J. Maps.*, 9, 289–298, doi:10.1080/17445647.2013.780188, 2013.
- Cevasco, A., Pepe, G. and Brandolini, P.: The influences of geological and land use settings on shallow landslides triggered by an intense rainfall event in a coastal terraced environment, *Bull. Eng. Geol. Environ.*, 73, 859–875, doi:10.1007/s10064-
480 013-0544-x, 2014.
- Cogan, J. and Gratchev, I.: A study on the effect of rainfall and slope characteristics on landslide initiation by means of flume tests, *Landslides*, 16(3), 2369-2378, doi:10.1007/s10346-019-01261-0, 2019.
- Crosta, G.B., Frattini, P.: Rainfall thresholds for triggering soil slips and debris flow. In: *Proc. 2nd EGS Plinius Conf. on Mediterranean Storms* (Mugnai A, Guzzetti F, Roth G, eds). Siena, pp. 463–487, 2001.
- 485 Cui, P., Zhu, Y.Y. and Chen, J.: Relationships between antecedent rainfall and debris flows in Jiangjia Ravine, China, In: *Proceedings of the Fourth International Conference on Debris Flow*, Chen, C.L., Rickenmann, D. Eds., Springer Press, Wellington, 1–9, 2008.
- Dai, F.C., Xu, C., Yao, X., Xu, L., Tu, X.B. and Gong, Q.M.: Spatial distribution of landslides triggered by the 2008 Ms 8.0 Wenchuan earthquake, China, *Journal of Asian Earth Sciences*, 40, 883-895, doi:10.1016/j.jseaes.2010.04.010, 2011.
- 490 De Vita, P., Napolitano, E., Godt, J.W. and Baum, R.L.: Deterministic estimation of hydrological thresholds for shallow landslide initiation and slope stability models: Case study from the Somma-Vesuvius area of southern Italy, *Landslides*, 10(6), 713-728, doi:10.1007/s10346-012-0348-2, 2012.
- Derbyshire, E., Asch, T. V., Billard, A. and Meng, X.: Modelling the erosional susceptibility of landslide catchments in thick loess: chinese variations on a theme by jan de ploey, *Catena*, 25(1–4), 315-331, doi:10.1016/0341-8162(95)00015-K, 1995.
- 495 Derbyshire, E.: Geological hazards in loess terrain, with particular reference to the loess regions of China, *Earth Science Reviews*, 54(1-3), 231-260, doi:10.1016/S0012-8252(01)00050-2, 2001.
- Dhakal, A.S. and Sidle, R.C.: Long-term modelling of landslides for different forest management practices, *Earth Surface Processes and Landforms*, 28(8), 853-868, doi:10.1002/esp.499, 2003.
- Di Napoli, M., Carotenuto, F., Cevasco, A., Confuorto, P., Di Martire, D., Firpo, M., Pepe, G., Raso, E. and Calcaterra, D.:
500 Machine learning ensemble modelling as a tool to improve landslide susceptibility mapping reliability, *Landslides*, 17, 1897–1914, doi:10.1007/s10346-020-01392-9, 2020.
- Di Napoli, M., Di Martire, D., Bausilio, G., Calcaterra, D., Confuorto, P., Firpo, M., Pepe, G. and Cevasco, A.: Rainfall-Induced Shallow Landslide Detachment, Transit and Runout Susceptibility Mapping by Integrating Machine Learning Techniques and GIS-Based Approaches, *Water*, 13(4), 488, doi:10.3390/w13040488, 2021.
- 505 Dijkstra, T.A., Rogers, C.D.F. and van Asch, T.W.J.: Cut slope and terrace edge failures in Malan loess, Lanzhou, PR China, In: *Proceedings of the XI ECSMFE conference*, Copenhagen, 61-67, 1995.

- Formetta, G., Capparelli, G. and Versace, P. Evaluating performance of simplified physically based models for shallow landslide susceptibility, *Hydrol. Earth Syst. Sci.*, 20, 4585–4603, doi:10.1016/j.enggeo.2009.12.004, 2016.
- Gabet, E.J. and Mudd, S.M.. The mobilization of debris flows from shallow landslides, *Geomorphology*, 74(1-4), 207-218, doi:10.1016/j.geomorph.2005.08.013, 2006.
- Galve, J.P., Cevasco, A., Brandolini, P. and Soldati, M.: Assessment of shallow landslide risk mitigation measures based on land use planning through probabilistic modelling, *Landslides*, 12, 101–114, doi:10.1007/s10346-014-0478-9, 2015.
- Giannecchini, R., Galanti, Y. and D'Amato, A.G.: Critical rainfall thresholds for triggering shallow landslides in the Serchio River Valley (Tuscany, Italy), *Nat Hazards Earth Syst Sci.*, 12, 828–842, doi:10.5194/nhess-12-829-2012, 2012.
- Giannecchini, R.: Relationship between rainfall and shallow landslides in the southern Apuan Alps (Italy), *Nat Hazards Earth Syst Sci.*, 6, 357–364, doi:10.5194/nhess-6-357-2006, 2006.
- Goetz, J.N., Brenning, A., Petschko, H. and Leopold, P.: Evaluating machine learning and statistical prediction techniques for landslide susceptibility modeling, *Comput. Geosci.*, 81, 1–11, doi:10.1016/j.trc.2015.03.039, 2015.
- Guadagno, F.M.: Debris flows in the Campanian volcanoclastic soil (Southern Italy). In: *Proc. Int. Conf. on slope stability. Isle of Wight: Thomas Telford*, pp. 125-130, 1991.
- Guo, W., Luo, L., Wang, W., Liu, Z., Chen, Z., Kang, H. and Yang, B.. Sensitivity of rainstorm-triggered shallow mass movements on gully slopes to topographical factors on the Chinese Loess Plateau, *Geomorphology*, 337, 69-78, doi:10.1016/j.geomorph.2019.04.006, 2019.
- Guo, X.J., Cui, P., Li, Y., Ma, L., Ge, Y.G. and William, B.M.. Intensity-duration threshold of rainfall-triggered debris flows in the Wenchuan Earthquake affected area, China, *Geomorphology*, 253, 208-216, doi:10.1016/j.geomorph.2015.10.009, 2016.
- Guo, X.J., Cui, P., Li, Y.: Debris flow warning threshold based on antecedent rainfall: A case study in Jiangjia Ravine, Yunnan, China, *Journal of Mountain Science*, 10(2), 305-314, doi: 10.1007/s11629-013-2521-z, 2013.
- Guzzetti, F., Galli, M., Reichenbach, P., Ardizzone, F. and Cardinali, M.: Landslide hazard assessment in the Collazzone area, Umbria, Central Italy, *Nat Hazards Earth Syst Sci.*, 6, 115–131, doi:10.5194/nhess-6-115-2006, 2006.
- Guzzetti, F., Malamud, B.D., Turcotte, D.L. and Reichenbach, P.. Power-law correlations of landslide areas in central Italy, *Earth Planet. Sci. Lett*, 195, 169-183, doi:10.1016/S0012-821X(01)00589-1, 2002.
- Guzzetti, F., Peruccacc, S., Ross, M. and Stark, C.P.. The rainfall intensity–duration control of shallow landslides and debris flows: an update, *Landslides*, 5, 3-17, doi:10.1007/s10346-007-0112-1, 2008.
- Guzzetti, F., Peruccacci, S., Rossi, M. and Stark, C.P.. Rainfall thresholds for the initiation of landslides in central and southern Europe, *Meteorol. Atmos. Phys*, 98, 239-267, doi:10.1007/s00703-007-0262-7, 2007.
- Harp, E.L. and Jibson, R.L.. Landslides triggered by the 1994 Northridge, California earthquake, *Bull. Seismol. Soc. Am.*, 86, S319–S332, doi:10.1029/95JB03253, 1996.
- Hungr, O., Evans, S.G., Bovis, M. and Hutchinson, J.N.. Review of the classification of landslides of the flow type, *Environ Eng Geosci*, 7, 221–238, doi:10.2113/gseegeosci.7.3.221, 2001.

- 540 Iverson, R.M., Reid, M.E. and LaHusen, R.G.: Debris-flow mobilization from landslide, *Annual Review of Earth and Planetary Sciences*, 25, 85-138, doi:10.1146/annurev.earth.25.1.85, 1997.
- Iverson, R.M.: Landslide triggering by rain infiltration, *Water Resour Res.*, 36(7), 1897-1910, doi:10.1029/2000WR900090, 2000.
- Jia, G., Yuan, T., Liu, Y. and Zhang, Y.: A static and dynamic factors-coupled forecasting model or regional rainfall-induced landslides: a case study of Shenzhen, *Sci China, Ser E.*, 51, 164-175, doi:10.1007/s11431-008-6013-2, 2008.
- 545 Jibson, R.W.: Debris flow in southern Porto Rico. Geological Society of America. special paper 236, 29-55, 1989.
- Juang, C.H., Dijkstra, T., Wasowski, J. and Meng, X.M.: Loess geohazards research in china: advances and challenges for mega engineering projects, *Engineering Geology*, 251, 1-10, doi:10.1016/j.enggeo.2019.01.019, 2019.
- Keles, F., Nefeslioglu, H. A. .: Infinite slope stability model and steady-state hydrology-based shallow landslide susceptibility evaluations: The Guneysu catchment area (Rize, Turkey)[J]., *Catena*, 200, 105161, doi: 10.1016/j.catena.2021.105161, 2021, 200.
- 550 Lade, P.V. and Duncan, J.M.: Elastoplastic Stress-Strain Theory for Cohesionless Soil, *J. Geotech. Eng.-ASCE*, 101, 1037-1053, doi:10.1016/0020-7683(77)90073-7, 1975.
- Leonarduzzi, E., Brian McArdell, W. and Molnar, P.: Rainfall-induced shallow landslides and soil wetness: comparison of physically based and probabilistic predictions, *Hydrol. Earth Syst. Sci.*, 25, 5937-5950, doi:10.5194/hess-2020-624, 2021.
- 555 Li, T.L., Long, J.H. and Li, X.S.: Types of loess landslides and methods for their movement forecast, *Journal of Engineering Geology*, 15(4),500-506, 2007. (in Chinese)
- Li, Y.R., Shi, W., Aydin, A., Beroya-Eitner, M.A. and Gao, G.H.: Loess genesis and worldwide distribution, *Earth-Science Reviews*, 201, 1-99, doi:10.1016/j.earscirev.2019.102947, 2019.
- 560 Lin, M.L. and Tung, C.C.: A GIS-based potential analysis of the landslides induced by the Chi-Chi earthquake, *Engineering Geology*, 71(1), 63-77, doi:10.1016/S0013-7952(03)00126-1, 2004.
- Liu, T.S.: *Loess and the Environment*; Science Press: Beijing, China, 1985. (in Chinese)
- Lizarraga, J.J., Frattini, P., Crosta, G B. and Buscarnera, G.: Regional-scale modelling of shallow landslides with different initiation mechanisms: sliding versus liquefaction, *Engineering Geology*, 228, 346-356, doi:10.1016/j.enggeo.2017.08.023, 565 2017.
- Lombardo, L., Opitz, T., Ardizzone, F., Guzzetti, F. and Huser, R.: Space-time landslide predictive modelling, *Earth Sci. Rev.*, 209, 103318, doi:10.1016/j.earscirev.2020.103318, 2020.
- Malamud, B.D., Turcotte, D.L., Guzzetti, F. and Reichenbach, P.: Landslides, earthquakes, and erosion, *Earth Planet. Sci. Lett.*, 229, 45-59, doi:10.1016/j.epsl.2004.10.018, 2004.
- 570 Marino, P., Peres, D.J., Cancelliere, A., Greco, R. and Bogaard, T.A. Soil moisture information can improve shallow landslide forecasting using the hydrometeorological threshold approach, *Landslides*, 17, 2041-2054, doi:10.1007/s10346-020-01420-8, 2020.

- Matsuoka, H. and Nakai, T.: Stress-Deformation and Strength Characteristics of Soil under Three Difference Principal Stresses, Proceedings of the Japan Society of Civil Engineers, 232, 59-70, doi:10.2208/jscej1969.1974.232_59, 1974.
- 575 Medina, V., Hürlimann, M., Guo, Z., Lloret, A., Vaunat, J.: et al. Fast physically-based model for rainfall-induced landslide susceptibility assessment at regional scale., CATENA, 201, 105213, doi: 10.1016/j.catena.2021.105213, 2021.
- Michel, J., Dario, C., Marc-Henri, D., Thierry, O. and Bejamin, R.. A review of methods used to estimate initial landslide failure surface depths and volumes, Engineering Geology, 267, 105478, doi:10.1016/j.enggeo.2020.105478, 2020.
- Montgomery, D.R. and Dietrich, W.E.: A physically based model for the topographic control on shallow landsliding, Water Resources Research, 30(4), 1153-1171, doi:10.1029/93WR02979, 1994.
- 580 Montrasio, L. and Valentino, R.: Experimental analysis and modelling of shallow landslides, Landslides, 4, 291–296, doi:10.1007/s10346-007-0082-3, 2007.
- Ochiai, H., Okada, Y., Furuya, G., Okura, Y., Matsui, T., Sammori, T., Terajima, T. and Sassa, K.. A fluidized landslide on a natural slope by artificial rainfall, Landslides, 1(3), 211-219, doi:10.1007/s10346-004-0030-4, 2004.
- 585 Owen, L.A., Kamp, U., Khattak, G.A.; Harp, E.L.; Keefer, D.K. and Bauer, M.A.. Landslides triggered by the 8 October 2005 Kashmir earthquake, Geomorphology, 94(1), 1-9, doi:10.1016/j.geomorph.2007.04.007, 2008.
- Pack, R.T., Tarboton, D.G. and Goodwin, C.N.: SINMAP 2.0-A Stability Index Approach to Terrain Stability Hazard Mapping, User's Manual. Terratech Consulting Ltd., Salmon Arm, Canada, 1999.
- Paronuzzi, P., Coccolo, A., Garlatti, G.: Eventi meteorici critical debris flows nei bacini montani del Friuli. L' Acqua, Sezione I=Memorie, pp, 39-50, 1998.
- 590 Peng, J.B., Fan, Z.J., Wu, D., Zhuang, J.Q., Dai, F.C., Chen, W.W. and Zhao, C.: Heavy rainfall triggered loess–mudstone landslide and subsequent debris flow in Tianshui, China, Engineering Geology, 186, 79-90, doi:10.1016/j.enggeo.2014.08.015, 2015.
- Peng, J.B., Zhuang, J.Q., Wang, G.H., Dai, F.C., Zhang, F.Y., Huang, W.L. and Xu, Q.. Liquefaction of loess landslides as a consequence of irrigation, Quarterly Journal of Engineering Geology and Hydrogeology, 51(3), 330-337, doi:10.1144/qjegh2017-098, 2018.
- 595 Preti, F.: Forest protection and protection forest: Tree root degradation over hydrological shallow landslides triggering, Ecological Engineering, 61(C): 633-645, doi: 10.1016/j.ecoleng.2012.11.009, 2013.
- Qi, T., Zhao, Y., Meng, X., Chen, G. and Dijkstra, T.. AI-Based Susceptibility Analysis of Shallow Landslides Induced by Heavy Rainfall in Tianshui, China, Remote Sensing, 13, 1819, doi:10.3390/rs13091819, 2021.
- 600 Reichenbach, P., Rossi, M., Malamud, B.D., Mihir, M. and Guzzetti, F.: A review of statistically-based landslide susceptibility models, Earth Sci. Rev., 180, 60-91, doi:10.1016/j.earscirev.2018.03.001, 2018.
- Rickli, C., Graf, F.: Effects of forests on shallow landslides – case studies in Switzerland, For. Snow Landsc. Res., 44, 33–44, 2009.

- 605 Roback, K., Clark, M.K., West, A.J., Zekkos, D., Li, G., Gallen, S.F., Chamlagain, D. and Godt, J.W.. The size, distribution, and mobility of landslides caused by the 2015 Mw 7.8 Gorkha earthquake, Nepal, *Geomorphology*, 301(15), 121-138, doi:10.1016/j.geomorph.2017.01.030, 2018.
- Roccati, A., Faccini, F., Luino, F., Turconi, L. and Guzzetti, F.: Rainfall events with shallow landslides in the Entella catchment, Liguria, Northern Italy, *Nat. Hazards Earth Syst. Sci.*, 18, 2367–2386, doi:10.5194/nhess-2017-432, 2018.
- 610 Roering, J.J., Schmidt, K.M., Stock, J.D., Dietrich, W.E., Montgomery, D.R.: Shallow landsliding, root reinforcement, and the spatial distribution of trees in the Oregon Coast Range, *Can. Geotech. J.*, 40, 237–253, 2003.
- Salciarini, D., Godt, J. W., Savage, W. Z., Conversini, P., Baum, R. L. and Michael, J. A.: Modeling regional initiation of rainfall-induced shallow landslides in the eastern Umbria region of central Italy, *Landslides*, 3, 181–194, doi:10.1007/s10346-006-0037-0, 2006.
- 615 Sassa, K. and Wang, G.H.: Mechanism of landslide-triggered debris flows: Liquefaction phenomena due to the undrained loading of torrent deposits, In: *Debris-flow hazards and related phenomena*, Springer, Berlin Heidelberg, 2005.
- Schilirò, L., Montrasio, L. and Mugnozza, G.S.: Prediction of shallow landslide occurrence: validation of a physically-based approach through a real case study, *Sci. Total Environ.*, 569–570, 134-144, doi:10.1016/j.scitotenv.2016.06.124, 2016.
- Segoni, S., Piciullo, L. and Gariano, S.L.: A review of the recent literature on rainfall thresholds for landslide occurrence. *Landslides*, 15, 1483–1501, doi:10.1007/s10346-018-0966-4, 2018.
- 620 Shieh, C.L., Chen, Y.S., Tsai, Y.J., Wu, J.H.: Variability in rainfall threshold for debris flow after the Chi-Chi earthquake in central Taiwan, China, *International Journal of Sediment Research*, 24(2), 177-188, doi: 10.1016/S1001-6279(09)60025-1, 2009.
- Skempton, A.W.: Residual strength of clays in landslides, folded strata and the laboratory, *Geotechnique*, 35(1), 3-18, doi:10.1680/geot.1985.35.1.3, 1985.
- 625 Stähli, M., Sättele, M., Huggel, C., McArdell, B.W., Lehmann, P., Van Herwijnen, A., Berne, A., Schleiss, M., Ferrari, A., Kos, A., Or, D. and Springman, S.M.: Monitoring and prediction in early warning systems for rapid mass movements, *Nat. Hazards Earth Syst. Sci.*, 15, 905–917, doi:10.5194/nhessd-2-7149-2014, 2015.
- Stark, C.P. and Hovius, N.: The characterization of landslide size distributions, *Geophys. Res. Lett.*, 28, 1091–1094, doi:10.1029/2000GL008527, 2001.
- 630 Sun, P., Li, R.J., Jiang, H., Igwe, O. and Shi, J.S.: Earthquake-triggered landslides by the 1718 Tongwei earthquake in Gansu Province, northwest China, *Bulletin of Engineering Geology and the Environment*, 76, 1281-1295, doi:10.1007/s10064-016-0949-4, 2017.
- Taylor, D.W.: *Fundamentals of soil mechanics*. LWW, 1948.
- 635 Thomas, M.A., Mirus, B.B. and Collins, B.D.: Identifying physics-based thresholds for rainfall-induced landsliding, *Geophys. Res. Lett.*, 45, 9651–9661, doi:10.1029/2018GL079662, 2018.

- Tu, X.B.; Kwong, A.K.L., Dai, F.C., Tham, L.G. and Min, H.: Field monitoring of rainfall infiltration in a loess slope and analysis of failure mechanism of rainfall-induced landslides, *Eng. Geol.*, 105, 134-150, doi:10.1016/j.enggeo.2008.11.011, 2009.
- 640 Van den Eeckhaut, M., Poesen, J., Govers, G., Verstraeten, G. and Demoulin, A.: Characteristics of the size distribution of recent and historical landslides in a populated hilly region, *Earth Planet. Sci. Lett.*, 256, 588-603, doi:10.1016/j.epsl.2007.01.040, 2007.
- von Ruetze, J., Papritz, A., Lehmann, P., Rickli, C. and Or, D.: Spatial statistical modeling of shallow landslides—validating predictions for different landslide inventories and rainfall events, *Geomorphology*, 133, 11–22, doi:10.1016/j.geomorph.2011.06.010, 2011.
- 645 Waldron, L.J.: The shear resistance of root-permeated homogeneous and stratified soil, *J. Soil Sci. Soc. Am.* 41, 843–849, doi: 10.2136/sssaj1977.03615995004100050005x, 1977.
- Wang, G. and Sassa, K.: Factors affecting rainfall-induced flowslides in laboratory flume tests, *Geotechnique*, 51(7), 587–599, doi:10.1680/geot.51.7.587.51386, 2001.
- 650 Wang, G.H.: An experimental study on the mechanism of fluidized landslide: with particular reference to the effect of grain size and fine-particle content on the fluidization behavior of sands, Phd. thesis, Kyoto University, Kyoto, 2000.
- Wang, G.L., Li, T.L., Xing, X.L. and Zou, Y.: Research on loess flow-slides induced by rainfall in July 2013 in Yan'an, NW China, *Environmental Earth Sciences*, 73(12), 7933-7944, doi:10.1007/s12665-014-3951-9, 2015.
- Wang, J.J., Liang, Y., Zhang, H.P., Wu, Y. and Lin, X.: A loess landslide induced by excavation and rainfall, *Landslides*, 11(1), 141–152, doi:10.1007/s10346-013-0418-0, 2014.
- 655 Wang, S., Zhang, K., van Beek, L. P., Tian, X. and Bogaard, T. A.: Physically-based landslide prediction over a large region: Scaling low-resolution hydrological model results for high-resolution slope stability assessment, *Environ. Model. Softw.*, 124, 104607, doi:10.1016/j.envsoft.2019.104607, 2020.
- Wieczorek, G.F.: Effect of rainfall intensity and duration on debris flows in central Santa Cruz Mountains. In: *Debris flow and avalanches: process, recognition, and mitigation* (Costa JE, Wieczorek GF, eds). Geological Society of America, *Reviews in Engineering Geology*, 7, 93–104, 1987,
- 660 Xu, L., Dai, F.C., Tham, L.G., Tu, X.B., Min, H., Zhou, Y.F. and Xu, K.: Field testing of irrigation effects on the stability of a cliff edge in loess, North-west China, *Engineering Geology*, 120, 10-17, doi:10.1016/j.enggeo.2011.03.007, 2011.
- Xu, L., Dai, F.C., Tu, X.B., Tham, L.G. and Zhou, Y.F.: Landslides in a loess platform, North-west China, *Landslides*, 11(6), 993-1005, doi:10.1007/s10346-013-0445-x, 2014,
- 665 Zhang, F.Y., Wang, G.H., Kamai, T., Chen, W.W., Zhang, D.X. and Yang, J.: Undrained shear behavior of saturated loess at different concentrations of sodium chloride solution, *Engineering Geology*, 155, 69-79, doi:10.1016/j.enggeo.2012.12.018, 2013.
- Zhang, M.S. and Liu, J.: Controlling factors of loess landslides in western China, *Environmental Earth Sciences*, 59(8), 1671-1680, doi:10.1007/s12665-009-0149-7, 2010.
- 670

- Zhang, Z.L., Wang, T. and Wu, S.R.: Distribution and features of landslides in the tianshui basin, northwest China, *J. Mt. Sci.* 17(3), 686-708, doi:10.1007/s11629-019-5595-4, 2020.
- Zhu, Y., Zhuang, J.Q., Zhao, Y.: Evaluation of loess-filled slope failure triggered by groundwater rise using a flume test, *Geomatics, Natural Hazards and Risk*, 13:1, 2471-2488, doi: org/10.1080/19475705.2022.2122592, 2022.
- 675 Zhuang J.Q., Ma, P.H., Zhan, J.W., Zhu, Y., Kong, J.X., Zhu, X.H., Leng, Y.Q. and Peng, J.B.: Empirical relationships of the landslides in the Chinese Loess Plateau and affect factors analysis, *Geomatics, Natural Hazards and Risk*, 13:1, 250-266, doi:org/10.1080/19475705.2021.2020174, 2022.
- Zhuang, J., Peng, C., Wang, G., Chen, X. Guo, X.: Rainfall thresholds for the occurrence of debris flows in the Jiangjia Gully, Yunnan Province, China, *Engineering Geology*, 195:335-346, doi: 10.1016/j.enggeo.2015.06.006, 2015.
- 680 Zhuang, J., Peng, J., Xu, C., Li, Z., Densmore, A., Milledge, D., Iqbal, J. and Cui, Y.: Distribution and characteristics of loess landslides triggered by the 1920 Haiyuan Earthquake, Northwest of China, *Geomorphology*, 314, 1-12, doi:10.1016/j.geomorph.2018.04.012, 2018.
- Zhuang, J.Q., Peng, J.B., Wang, G.H., Javed, I., Wang, Y. and Li, W.: Distribution and characteristics of landslide in Loess Plateau A case study in Shaanxi province, *Engineering Geology*, 236, 89-96, doi:10.1016/j.enggeo.2017.03.001, 20108.
- 685 Zhuang, J.Q., Peng, J.B., Wang, G.H., Javed, I., Wang, Y. and Li, W.: Prediction of rainfall-induced shallow landslides in the Loess Plateau, Yan'an, China, using the TRIGRS model, *Earth Surface Processes and Landforms*, 42(6), 915-927, doi:10.1002/esp.4050, 2017.
- Zizioli, D., Meisina, C., Valentino, R. and Montrasio, L.: Comparison between different approaches to modelling shallow landslide susceptibility: a case history in Oltrepo Pavese, Northern Italy, *Nat Hazards Earth Syst Sci.*, 13, 559-573, 690 doi:10.5194/nhess-13-559-2013, 2013.